


Article

Chemical and Structural Characterization of Sandblasted Surface of Dental Implant using ZrO₂ Particle with Different Shape

Oleg Mishchenko ^{1,2}, Vira Filatova ³, Mykhaylo Vasylyev ³, Volodymyr Deineka ⁴ and Maksym Pogorielov ^{1,4,*} 

¹ Osteoplast R&D, 25 Metalowcow Str., Dedice 39-200, Poland; Dr.Mischenko@i.ua

² Department of Surgical and Propaedeutic Dentistry, Zaporizhzhia State Medical University, 26, Prosp.Mayakovskogo, 69035 Zaporizhzhia, Ukraine

³ G.V. Kurdyumov Institute for Metal Physics of the N.A.S. of Ukraine, 36 Vernadsky Av., 03142 Kyiv, Ukraine; Filatova@nas.gov.ua (V.F.); Vasylyev@nas.gov.ua (M.V.)

⁴ Medical Institute, Sumy State University, 2 R-Korsakova Str, 40007 Sumy, Ukraine; vovadeineka@gmail.com

* Correspondence: m.pogorielov@gmail.com; Tel.: +38-066-900-54-48

Received: 18 January 2019; Accepted: 26 March 2019; Published: 28 March 2019



Abstract: The clinical success of dental implantation is associated with the phenomenon of osteointegration. Geometry and topography of the implant surface are critical for the short- and long-term success of an implantation. Modification of the surface of endosseous part of the implant with sandblasting was of special interest for our study. Taking into account the advantages of currently used ceramic abrasives: aluminum oxide, titanium oxide, calcium phosphate, these materials are able to break down during collision with the treated surface, the possibility of incorporation of their residues into the implant surface, as well as the difficulty of removing these residues. This paper aimed to determine the preferred composition and the shape of the abrasive, as well as the treatment regime for ZrO₂ sandblasting modification of the surface of the endosseous part of the dental implant. Tetragonal and cubic solid solutions are based on ZrO₂, as an abrasive that is applied for zirconium-niobium alloy sandblasting under different pressures. Optical and scanning electron microscopy, the physical and chemical state of the surface of implants as well as contact angle measurement and cell viability were used to assess surface after sandblasting. The results demonstrate the potential of using granular powders that are based on zirconium dioxide as an abrasive to create a rough surface on endosseous part of dental implants made from zirconium-based alloys. It does not lead to a significant change in the chemical composition of the surface layer of the alloy and it does not require subsequent etching in order to remove the abrasive particles. Based on structural and chemical characterization, as well as on cell viability and contact angle measurement, sandblasting by tetragonal ZrO₂ powder in 4 atm. and an exposure time of 5 s provided the best surface for dental implant application.

Keywords: dental implant; surface treatment; sandblasting; ZrO₂

1. Introduction

Over the past 20 years, the number of placed dental implants in the world has reached about one-million a year. Clinical success of dental implantation is associated with the phenomenon of osteointegration. Geometry and topography of the implant surface are critical for the short- and long-term success of an implantation. These parameters, in combination with flawless surgical techniques, are a necessary condition for obtaining a successful clinical outcome [1].

There are two types of reaction of bone tissue on the implant. The first type involves the formation of a fibrous soft capsule around the implant. This capsule, which consists of fibrous tissue, does not provide proper biomechanical fixation and it leads to clinical failure of the dental implant. Direct contact of the implant and bone surfaces without an intermediate layer of connective tissue characterizes the second type of bone reaction. This phenomenon is known as osteointegration. Change in the microstructure of the implant surface has been the goal of numerous studies in recent years, especially with the advent of a variety of methods to refine the grain size of these materials down to the submicron range/nano. The development of these techniques made it possible to create a surface with exceptional mechanical properties [2–4] and enhanced biological compatibility [5–8]

The rate and quality of osteointegration of implants are known to be related to their surface properties. Composition, hydrophilicity, and roughness are the parameters that can play a certain role in the interaction of the implant with surrounding tissues.

There are numerous studies proving that the surface roughness of implants affects the rate of osteointegration and biomechanical fixation [9,10]. The surface roughness can be divided into three levels, depending on the scale: macro-, micro-, and nanoscale topologies. The macrolevel assumes a surface structure with an interval of variations in the range up to tens of microns. This scale directly determines the implant geometry. Numerous studies have shown that the primary fixation and long-term mechanical stability of the implant can be improved by means of the developed surface geometry [11–13]. The microlevel of the implant surface is determined in the range of 1–10 μm . This roughness range regulates the connection between the bone tissue and the implant surface [10,13]. In cases of insufficient bone tissue, short implants, which were developed with a rough surface, showed superior clinical results when compared to the implants with a smooth surface [14,15]. Numerous studies have shown that the surface roughness in this range provides a stable implant integration and a higher torque resistance when the implant is being unscrewed when compared to the other types of surface geometry [10,13]. These studies have established that implants with rough surfaces have greater contact with the bone as compared to the implants with a smoother surface [9,10]. Nevertheless, to date, no clinical signs have been revealed that demonstrate the superiority of any particular implant surface geometry [16].

Up to date, various methods for modifying the surface of dental implants have been developed in order to improve their osteointegration. These methods use plasma action, sandblasting with ceramic particles, acid etching, and anodizing.

Modification of the surface of endosseous part of the implant with sandblasting was of special interest for our study. The method is based on the impact of the implant surface with solid ceramic particles that are projected through the nozzle at high speed with compressed air. Depending on the size, characteristics of ceramic particles, and modes of their projection, surfaces with different characteristics can be obtained. At the same time, the abrasive should be chemically stable, biocompatible, and it should not interfere with the osteointegration of the implants. There are the following ceramic abrasives: aluminum oxide, titanium oxide, and calcium phosphate. The disadvantages of the listed materials are their ability to break down during collision with the treated surface, the possibility of incorporation of their residues into the implant surface, as well as the difficulty of removing these residues, even by means of ultrasonic cleaning, acid passivation, and sterilization. Aluminum oxide does not dissolve in acid and it is thus difficult to remove from the implant surface. Cases of migration of abrasive particles into surrounding tissues and their interference with the processes of osteointegration of implants have been reported. The presence of abrasive residues on the surface of the implant disrupts its chemical heterogeneity, which reduces the corrosion resistance in the environment [17]. Titanium oxide is also used for sandblasting of the surface of implants. Titanium oxide particles with an average size of 25 μm produce a moderately uneven surface of 1–2 μm . Experimental studies of microimplants in the human body showed higher osteoconductive abilities of surfaces that were treated with TiO_2 when compared to other abrasives [12,18–21]. In an experiment with rabbits, Wennerberg et al. [13] proved that the impact

of TiO₂ or Al₂O₃ particles on the implant surface yielded similar bone regeneration values [22]. These studies also confirm that the modification of the implant surface with the creation of a roughness increases their mechanical fixation in the bone.

Despite the existence of a sufficient number of methods and technologies for surface treatment, the creation of a developed surface of the endosseous part of the implant remains an important task [23]. Since each method has its advantages and disadvantages, the search for the methods to improve the technology in order to enhance the biocompatibility of implants continues.

The aim of this paper was to determine the preferred composition and shape of the abrasive, as well as the treatment regime for ZrO₂ sandblasting modification of the surface of the endosseous part of the dental implant.

2. Materials and Methods

2.1. Materials

The KTZ-125 alloy of the zirconium-niobium system (Zr–2.5 wt.% Nb) that was obtained from Osteoplast R&D (Dębica, Poland) we used in experiment. 7 mm diameter cylindrical samples with a height of 3 mm were prepared for sandblasting. Before processing, the samples were subjected to mechanical grinding and polishing. Tetragonal (T-ZrO₂) and cubic (C-ZrO₂) zirconium dioxide granules with a fraction size of 250 μm were used as a sandblasting agent (prepared in Institute for Problems in Materials Science, Kyiv, Ukraine). The granules were obtained from a nanocrystalline zirconium dioxide powder, which was complexly stabilized with yttrium and cerium oxides (ZrO₂–Y₂O₃–CeO₂).

All media and reagents for the cell culture experiment were purchased from Gibco[®], USA (Gaithersburg, MD). Primary cultures of Human osteoblast were obtained from medical company Ilaya (Kyiv, Ukraine).

2.2. Sandblasting Process

Abrasive treatment of the surface was carried out in the Heraeus Combilabor Kulzer CL-FSG94 chamber. Nozzle diameter of the sandblast gun was 1.2 mm, the air pressure was 4 and 6 atm, the distance from the nozzle to the sample surface was 1.3 cm, and the bombardment angle was 90°. The processing time equaled 5 s.

2.3. Alloy Chemical Compound

X-ray fluorescent analysis (XRF, Carl Zeiss, Oberkochen, Germany), using a VRA-20 spectrometer, was used to determine the surface chemical composition before and after sandblasting treatment.

2.4. Surface Erosion Assessment

To assess erosive wear (*Er*), all of the samples were weighed before and after treatment and formula 1 was used:

$$Er = \frac{M_i}{S} - \frac{M_p}{S} \quad (1)$$

where, *M_i*—initial sample weight, mg; *M_p*—posttreatment sample weight, mg; *S*—sample area, cm².

2.5. Optical Microscopy

To visualize the geometric shape of the abrasive and to evaluate its effect on the surface of the alloy samples, the Zeiss Axiovert 40 optical microscope (Zeiss, Oberkochen, Germany) was used, with 50×, 100×, and 200× magnification. An analysis of the distribution of implanted particles was carried out while using Image Jay image processing software (V 2.0).

2.6. Scanning Electron Microscopy

Scanned Electron Microscope Tescan Mira 3LMN (Tescan, Czech Republic) was used to analyze the surface morphology after treatment and chemical composition. Secondary (surface geometry mode) and reflected (phase contrast mode) electrons mode were applied. In the surface survey mode, the accelerating voltage for determining the topography was 10 keV, the electron beam current was 10 A, and the beam diameter was 0.03 μm . In this case, the magnification was set at 500–30000 times. The chemical analysis of the surface was carried out using an EDS Oxford X-max 80 mm² energy dispersive analyzer (EDA) (Oxford-instruments, Oxford, UK), at an accelerating voltage of 20 keV.

2.7. Surface Roughness Measurement

The R_a values were determined using Mahr profilometer (Mahr GmbH, Göttingen, Germany). Before measurement, all of the samples washed in 96% ethanol in Emmi-20HC ultrasonic bath (EMAG, Mörfelden-Walldorf, Germany). Measurement length was 1.5 mm and it was carried out in triplicate.

2.8. Contact Angle Measurement

Contact angle (CA) measurements experiments were made using a video-based optical contact angle measuring instrument (OCA 15 EC, Data Physics, San Jose, CA, USA). The CA data was recorded for ultra-pure water, for at least three parallel samples.

2.9. Cell Culture Experiment

Samples before and after sandblasting (six in each group) being 10 mm in diameter were sterilized by 70% ethanol for 3 h at room temperature, washed in PBS twice, and then placed in 24-well plates. Dulbecco's Modified Eagle Medium/Nutrient Mixture F-12 (DMEM/F-12) with L-glutamine used, containing 100 units/mL penicillin, 100 $\mu\text{g}/\text{mL}$ streptomycin, 2.5 $\mu\text{g}/\text{mL}$ amphotericin B, 10% Fetal Bovine Serum, and 1.0 ng/mL bFGF was added to each well, and it was then incubated at 37 °C in a humidified environment with 5 % CO₂. After 24 h, the human osteoblast cells were seeded at 10⁴ cells per sample in 2 mL of DMEM/F-12. Samples with cells were incubated at 37 °C with 5% CO₂, and media was changed every two days during a seven-day culture period. All of the experiments were triplicates.

Alamar Blue (AB) assay was used to access cell viability on day one, three, and seven after seeding. The media was removed from each well and washed with PBS. 1 mL of Alamar Blue™ solution was added to each scaffold and then incubated for two hours. Two aliquots of 200 μL of Alamar Blue™ solution were collected from each scaffold and the absorbance was read on the absorbance reader using 570 and 600 nm wave lengths.

2.10. Statistic

Data was expressed as means \pm standard deviation. Student's *t*-test on unpaired data was used to assess the statistical significance of the difference. Statistical significance was assumed at a confidence level of 95% ($p < 0.05$).

3. Results and Discussion

3.1. Optical Microscopy

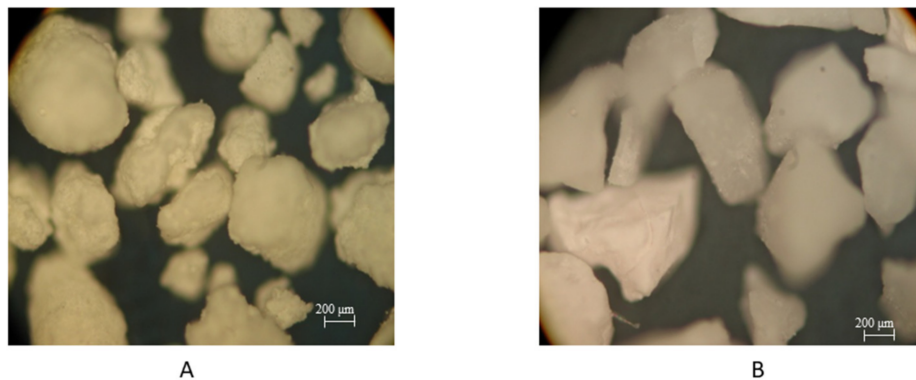
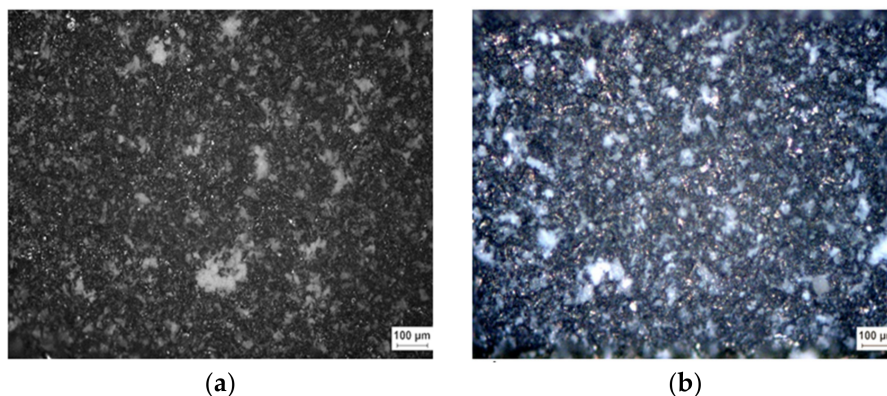
As described above, for the sandblasting process, we have used two types of ZrO₂ abrasives—tetragonal and cubic shape. In Table 1, individual physical characteristics of the abrasives are shown.

Table 1. Comparative characteristics of abrasives.

Characteristic	Abrasive	
	ZrO ₂ Tetragonal	ZrO ₂ Cubic
Density, g/cm ³	6.0–6.05	6.5–10
Modulus of rupture in bending, MPa	750–1050	–
Young's modulus, GPa	200–210	–
Vickers hardness, GPa	12–13	–
Crack resistance, MPa m ^{1/2}	8.0–10.0	–
Moh's hardness	–	7.5–8.5

Optical microscopy of ZrO particles show (Figure 1) that the abrasive based of T-ZrO₂ has a rounded shape with small sharp protrusions over the entire surface, and the C-ZrO₂ particles have sharp edges and an uneven surface. Based on mechanical and morphological parameters, they can provide different effects to implant surface within the sandblasting surface.

The surface characteristics, as well as particle distribution after sandblasting using ZrO abrasive, depends on particle shape and applied pressure. The implantation of abrasive particles of up to 50–100 µm in size is typical for all samples after sandblasting. However, the increasing of pressure from 4 to 6 atm during the sandblasting leads to single implantation of 200 µm particles for both types of abrasive. Alloy treatment with T-ZrO₂ powder at a pressure of 4 atm lead to covering 24% of the surface with abrasive particles (Figure 2a). However, if pressure increase up to 6 atm, the particle distribution decreases—only 17% of surface covered by ZnO particle. For C-ZrO₂ powder, we determine opposite dependence—increasing of pressure lead to an increasing of particle distribution from 14% to 29% (Figure 2c,d).

**Figure 1.** Optical microscopy image of T-ZrO₂ (A) and C-ZrO₂ (B) particle, used for sandblasting. ×1000.**Figure 2.** Cont.

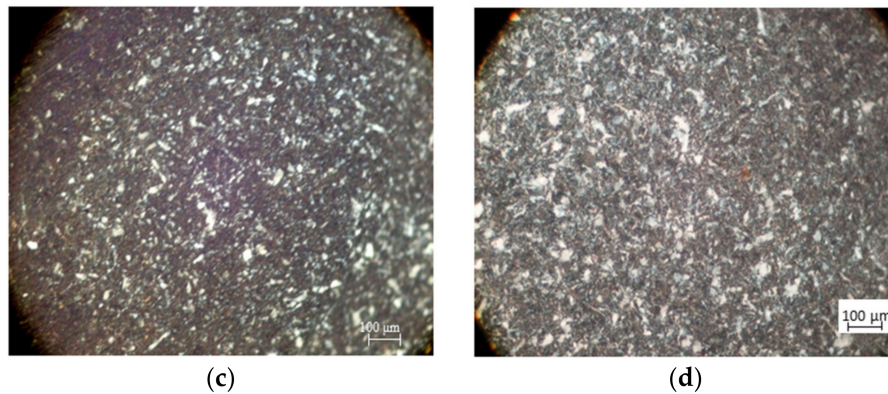


Figure 2. Optical microscopy image of sandblasted surface using T-ZrO₂ particles ((a) 4 atm; (b) 6 atm) and C-ZrO₂ ((c) 4 atm; (d) 6 atm) ×200.

3.2. Chemical Composition of the Surface after Treatment

The integrated surface chemical composition was determined as the average value at the three selected areas. Data indicates a uniform trend towards oxygen wt.% increasing in the samples that were treated with ZrO₂ particles. It can notify (Figure 3a) an increase in the oxygen wt.% upon treatment with both types of ZrO₂ abrasives. A noticeable decrease of the content of basic elements of the zirconium and niobium alloy in the surface layer indicates an increase in the thickness of the modified surface region. At the same time, the oxygen content increases to 20 wt.%, which can probably indicate the formation of a dense oxide film or additional incorporation of O after sandblasting using ZrO₂. The application of T-ZrO₂ powder leads to an increasing of oxygen wt.% up to 23% as compared to the C-ZrO₂. The local chemical composition analysis was carried out at selected areas in order to identify the inclusion phases. Figure 3b shows the different types of surface areas of the sample after treatment with T-ZrO₂ powder and areas of chemical analysis; the results of which are presented in Figure 3c. Local analysis allows for identifying inclusions of abrasive particles (Spectrum 1), contamination (Spectrum 2), and areas of the alloy surface, which were not significantly affected (Spectrum 3).

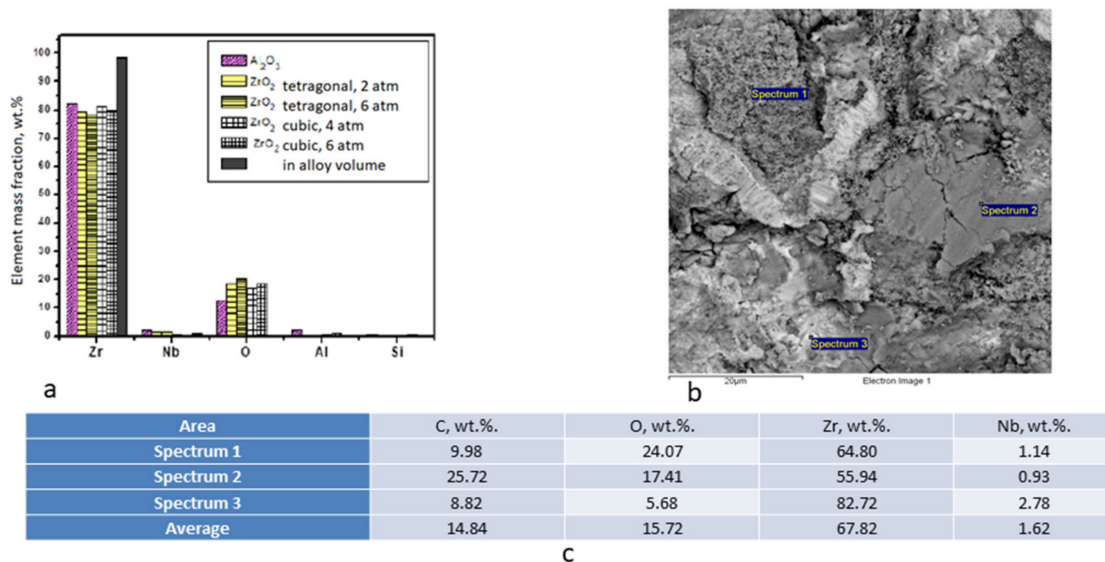


Figure 3. Chemical composition of the surface layer of alloy depending on the type of abrasive and treatment mode. (a)—X-ray fluorescent analysis. (b)—Chart of chemical analysis of the surface areas of a sample treated with T-ZrO₂ at a pressure of 6 atm and (c)—EDX from selected areas (from (b)).

3.3. Scanning Electron Microscopy

Surface analysis in the secondary electron mode allows for observing the contrast in height, since dark spots correspond to basins, and bright spots correspond to elevations (Figure 4). After alloy treatment with T-ZrO₂ powder, a developed surface with lacunae and protrusions of about 50 μm is formed. However, at high magnification, it should be noticed that pores of about 0.5 μm formed on the surface after treatment at a pressure of 4 atm are destroyed when the pressure increases up to 6 atm (Figure 4c). Obviously, particles have a higher velocity and most of the particles interact with the front side not perpendicularly, but tangentially, and such particles leave the corresponding traces on the surface.

The effect of C-ZrO₂ abrasive to sample surface is similar to that of the T-ZrO₂ ones (Figure 4b,d). During a detailed study of structure, the formation of regular structures 0.5 μm in size is noticeable, but along with this, traces of large-sized powder particles interacting with the surface at a tangent are also visible (Figure 4b). When pressure increases, such structures are no longer formed, evidently because of the high interaction energy (Figure 4d).

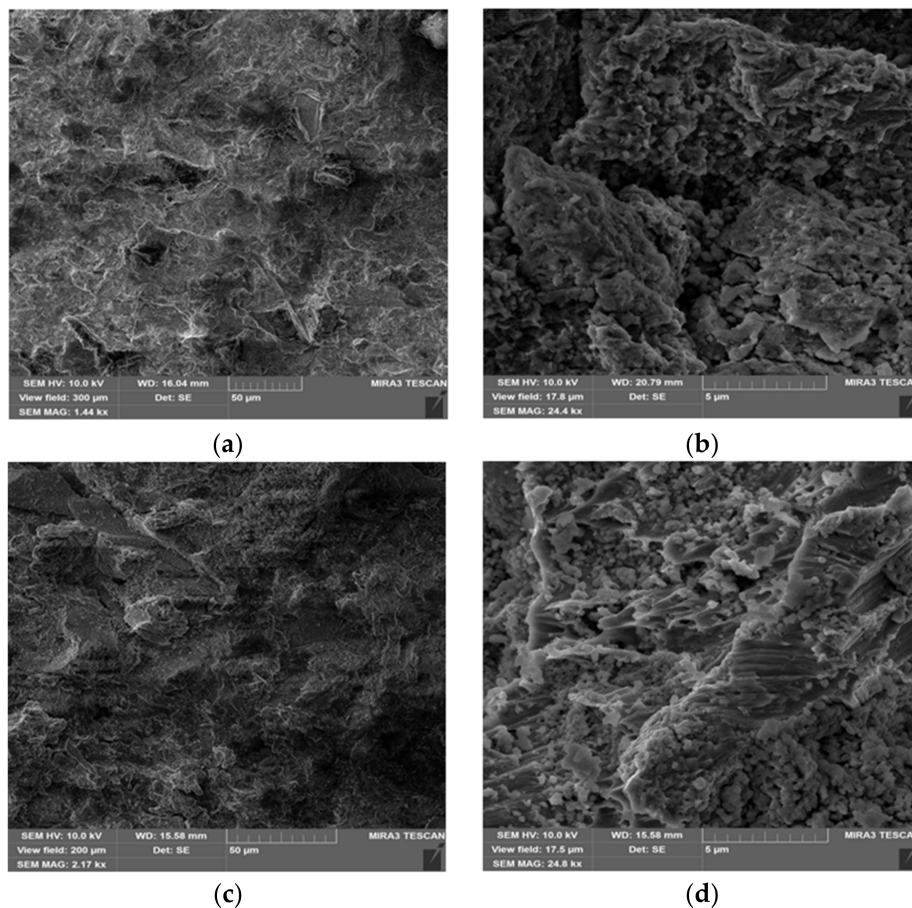


Figure 4. Scanning electron microscopy of samples after sandblasting using T-ZrO₂ powder (a,c) and C-ZrO₂ powder (b,d) in different regimen: (a,b)—5 sec with pressure of 4 atm, (c,d)—5 sec with pressure of 6 atm.

3.4. Contact Angle and Roughness

Average R_a values in all experimental groups significantly increased when compared to the polished ones. There were no differences between pressure used for the sandblasting process. The C-ZrO₂ particle provided significant less roughness when compared to the T-ZrO₂ ones (Table 2).

The CA of polished surface was $92.17^\circ \pm 2.78^\circ$ and it significantly decreased in both T-ZrO₂ ($76.83^\circ \pm 2.63^\circ$ and $82.13^\circ \pm 5.10^\circ$) and in C-ZrO₂ treated under the 4 atm. ($81.17^\circ \pm 4.66^\circ$). Cubic

ZrO₂ powder application under 6 atm. leads to not significant decrease of CA of up to $86.5^\circ \pm 3.20^\circ$ ($p = 0.10$). There were no significant differences in CA between samples that were treated in different atm. with same ZrO₂ shapes.

Table 2. R_a values (μm) and CA ($^\circ$) measurement results after treatment with different particle shape and time.

Parameter	Polished	ZrO ₂ Tetragonal		ZrO ₂ Cubic	
		4 atm	6 atm	4 atm	6 atm
R_a Values (μm)	0.45 ± 0.092	3.57 ± 0.12	3.86 ± 0.35	2.19 ± 0.28	2.76 ± 0.44
CA ($^\circ$)	92.17 ± 2.78	76.83 ± 2.63	82.13 ± 5.10	81.17 ± 4.66	86.5 ± 3.20

3.5. Cell Culture

The cell viability assay did not show cell toxicity of all surfaces, but the attachment and proliferation rates were significantly different, depending on groups. When comparing the positive control—Tissue culture plastic (TCP), cell attachment rate (percent of viable cells) on day 1 was significantly ($p \leq 0.001$) less on the polished non-modified ZrNb surface. The surface that was sandblasted by T-ZrO₂ particles shows significant more cell viability than the polished ($p \leq 0.001$) and C-ZrO₂ ones ($p = 0.023$). We did not see any significant differences in cell number between samples that were treated in 4 and 5 atm. (Figure 5A).

On day 3 and 7, we observed cell proliferation in all samples, but osteoblast better proliferate on sandblasted surfaces (Figure 5B,C). The minimal cells were detected on the polished surface due to low attachment on day 1. Both time-point did not show differences in cell viability between the TCP and T-ZrO₂ surfaces. It should be noted that on day 7 that osteoblast proliferated much better with significant difference ($p \leq 0.01$) on T-ZrO₂ compare the C-ZrO₂ with no difference within samples that were treated in 4 and 5 atm.

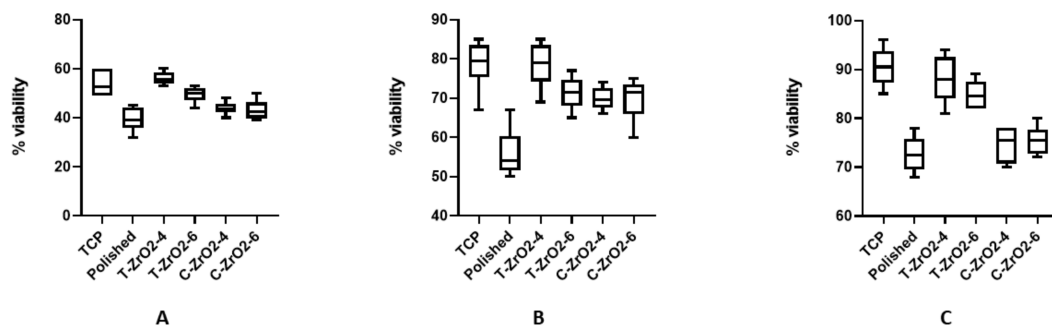


Figure 5. Cell viability assay of human osteoblasts on different surfaces on day 1 (A), 3 (B) and 7 (C); $N = 3$.

4. Discussion

Surface topography and chemistry are essential parameters for the interaction between implant and surrounding tissues due to their influence on ion exchange, protein adsorption, and cell adhesion and interaction. There are a lot of evidences that rough surfaces significantly increase the osteogenic properties of different materials [24]. Surface topography is a key factor for successful metal-tissue integration. The process of direct anchorage of an implant by the formation of bony tissues around the implant without the growth of fibrous tissues at the bone/implant interface is the osteointegration [25]. This process starts directly after the implantation from blood protein and growth factors absorption on implant surface with further cell attachment and proliferation [26]. Bone progenitor cells, like mesenchymal stem cells (MSCs) and lining osteoblast, produce collagen with further mineralization and bone remodeling. In this paradigm, surface topography and wettability are key parameters in determining implant/tissue interaction and osteointegration [27].

The design of surfaces with high waviness and porosity in microscale dimensions allows for bone ingrowth and induces strong bone interlocking, thereby improving the mechanical resistance and stability of the implant [28]. Various treatments have been developed to modify the implants surface, including machining/micromachining, sand-blasting, acid etching, electropolishing, anodic oxidation, and plasma spraying [29].

Surface stability after treatment is a key factor of clinical success. Some authors [30] found that most of the failed implants are characterized by an affected surface, on which a large number of embedded microparticles of Al_2O_3 , as well as rare-earth oxides, were detected. Moreover, titanium and aluminum ions were found in the bone matrix.

In this paper we assessed possible application of ZrO_2 powder in cubic and tetragonal shape for ZrNb-based implant sandblasting in different regimen—4 and 6 atm. The main attention was paid to the complex stabilization of zirconium dioxide with yttrium and cerium oxides. This is necessary to prevent the “aging” process, i.e., the destruction of bioinert ZrO_2 -based materials in a living organism due to uncontrolled phase transformation of tetragonal ZrO_2 modification into a monoclinic ZrO_2 modification in moist environment [31].

Our data have shown that the application of ZrO_2 in both shapes did not affect chemical composition of implant but add some additional oxygen, which is probably due to the incorporation of ZrO_2 . Chemical interaction of the metal with the abrasive, a strong adherence of particles to the surface layer, and additional surface oxidation are observed in the surface layers that are activated in such a way [23,32].

Sandblasting using ZrO_2 powder in a tetragonal shape significantly decrease the contact angle of implant that is one of critical factor of osteointegration. Hydrophilic (CA less than 90°) surface can provide more better protein absorption after the implantation procedure. The cell culture experiment supports this data and has shown better cell adhesion and proliferation on a sandblasted surface, spatially on substrate that is treated by tetragonal shape ZrO_2 .

5. Conclusion

- The results demonstrate the potential of using granular powders that are based on zirconium dioxide as an abrasive to create a rough surface with a low contact angle; also being absent of cell toxicity on the endosseous part of dental implants made from zirconium-based alloys.
- Sandblasting with the abrasive, as proposed in this paper, does not lead to a significant change in the chemical composition of the surface layer of the alloy and it does not require subsequent etching in order to remove abrasive particles, as in the case of a traditional abrasive on the basis of aluminum oxide, which should have a positive effect on the corrosion characteristics of the implants (biocompatibility).
- It was found that it is preferable to use round shaped powder of ZrO_2 pellets of tetragonal form, with small sharp protrusions over the entire surface, with a size of $250\ \mu\text{m}$, at an operating pressure of not more than 4 atm and an exposure time of 5 s.

Author Contributions: Conceptualization, O.M.; Methodology, O.M., V.F., V.D. and M.V.; Software, O.M., V.F., V.D. and M.V.; Investigation, O.M., V.F. and M.P.; Data Curation, O.M., V.F. and M.P.; Writing—Original Draft Preparation, O.M.; Writing—Review and Editing, M.P.; Supervision, M.P.

Funding: This research was funded by H2020 Marie Skłodowska-Curie Actions (NanoSurf 777926) and partly by project POIR.01.01.02-00-0022/16. Pt. “Development of technology and launching the production of innovative dental implants with increased osteoinductive properties”.

Conflicts of Interest: The authors declare no conflict of interest.

References

1. Albrektsson, T.; Branemark, P.I.; Hansson, H.A.; Lindstrom, J. Osseointegrated titanium implants. Requirements for ensuring a long-lasting, direct bone-to-implant anchorage in man. *Acta Orthop. Scand.* **1981**, *52*, 155–170. [[CrossRef](#)]
2. Estrin, Y.; Vinogradov, A. Extreme grain refinement by severe plastic deformation: A wealth of challenging science. *Acta Materialia* **2013**, *61*, 782–817. [[CrossRef](#)]
3. Valiev, R.Z.; Sabirov, I.; Zhilyaev, A.P.; Langdon, T.G. Bulk Nanostructured Metals for Innovative Applications. *JOM* **2012**, *64*, 1134–1142. [[CrossRef](#)]
4. Valiev, R.Z.; Alexandrov, I.V.; Zhu, Y.T.; Lowe, T.C. Paradox of strength and ductility in metals processed by severe plastic deformation. *J. Mater. Res.* **2002**, *17*, 5–8. [[CrossRef](#)]
5. Bindu, S.; Sanosh, K.P.; Balakrishnan, A.; Kim, T.N. An in vivo evaluation of ultra-fine grained titanium implants. *J. Mater. Sci. Technol.* **2009**, *25*, 556–560.
6. Estrin, Y.; Ivanova, E.P.; Michalska, A.; Truong, V.K.; Lapovok, R.; Boyd, R. Accelerated stem cell attachment to ultrafine grained titanium. *Acta Biomaterialia* **2011**, *7*, 900–906. [[CrossRef](#)] [[PubMed](#)]
7. Estrin, Y.; Kasper, C.; Diederichs, S.; Lapovok, R. Accelerated growth of preosteoblastic cells on ultrafine grained titanium. *J. Biomed. Mater. Res. A* **2009**, *90*, 1239–1242. [[CrossRef](#)]
8. Valiev, R.Z.; Semenova, I.P.; Latysh, V.V.; Rack, H.; Lowe, T.C.; Petruzelka, J.; Dluhos, L.; Hrusak, D.; Sochova, J. Nanostructured titanium for biomedical applications. *Adv. Eng. Mater.* **2008**, *10*, B15–B17. [[CrossRef](#)]
9. Cochran, D.L.; Schenk, R.K.; Lussi, A.; Higginbottom, F.L.; Buser, D. Bone response to unloaded and loaded titanium implants with a sandblasted and acid-etched surface: A histometric study in the canine mandible. *J. Biomed. Mater. Res.* **1998**, *40*, 1–11. [[CrossRef](#)]
10. Wennerberg, A.; Hallgren, C.; Johansson, C.; Danelli, S. A histomorphometric evaluation of screw-shaped implants each prepared with two surface roughnesses. *Clin. Oral Implant. Res.* **1998**, *9*, 11–19. [[CrossRef](#)]
11. Buser, D.; Schenk, R.K.; Steinemann, S.; Fiorellini, J.P.; Fox, C.H.; Stich, H. Influence of surface characteristics on bone integration of titanium implants. A histomorphometric study in miniature pigs. *J. Biomed. Mater. Res.* **1991**, *25*, 889–902. [[CrossRef](#)]
12. Gotfredson, K.; Wennerberg, A.; Johansson, C.; Skovgaard, L.T.; Hjørtting-Hansen, E.; Hjørtting-Hansen, E. Anchorage of TiO₂-blasted, HA-coated, and machined implants: An experimental study with rabbits. *J. Biomed. Mater. Res.* **1995**, *29*, 1223–1231. [[CrossRef](#)]
13. Wennerberg, A.; Albrektsson, T.; Albrektsson, B.; Krol, J.J. Histomorphometric and removal torque study of screw-shaped titanium implants with three different surface topographies. *Clin. Oral. Implants Res.* **1996**, *6*, 24–30. [[CrossRef](#)]
14. Testori, T.; Wiseman, L.; Woolfe, S.; Porter, S.S. A prospective multicenter clinical study of the Osseotite implant: Four-year interim report. *Int. J. Oral Maxillofac. Implant.* **2001**, *16*, 193–200.
15. Conner, K.A.; Sabatini, R.; Mealey, B.L.; Takacs, V.J.; Mills, M.P.; Cochran, D.L. Guided Bone Regeneration Around Titanium Plasma-Sprayed, Acid-Etched, and Hydroxyapatite-Coated Implants in the Canine Model. *J. Periodontol.* **2003**, *74*, 658–668. [[CrossRef](#)]
16. Coulthard, P.; Thomsen, P.; Worthington, H.V. Interventions for replacing missing teeth: Different types of dental implants. *Cochrane Database Syst. Rev.* **2005**, *25*, CD003815.
17. Aparicio, C.; Gil, F.J.; Fonseca, C.; Barbosa, M.; Planell, J.A. Corrosion behavior of commercially pure titanium shot blasted with different materials and size of shot particles for dental implant applications. *Biomaterials* **2003**, *24*, 263–273. [[CrossRef](#)]
18. Ivanoff, C.-J.; Widmark, G.; Hallgren, C.; Sennerby, L.; Wennerberg, A. Histologic evaluation of the bone integration of TiO₂ blasted and turned titanium microimplants in humans. *Clin. Oral Implant. Res.* **2001**, *12*, 128–134. [[CrossRef](#)]
19. Rasmusson, L.; Kahnberg, K.-E.; Tan, A. Effects of Implant design and surface on bone regeneration and implant stability: An experimental study in the dog mandible. *Clin. Implant. Dent. Relat. Res.* **2001**, *3*, 2–8. [[CrossRef](#)]
20. Gotfredsen, K.; Karlsson, U. A prospective 5-year study of fixed partial prostheses supported by implants with machined and TiO₂-blasted surface. *J. Prosthodont.* **2001**, *10*, 2–7. [[CrossRef](#)]

21. Rasmusson, L.; Roos, J.; Bystedt, H. A 10-year follow-up study of titanium dioxide-blasted implants. *Clin. Implant. Dent. Relat. Res.* **2005**, *7*, 36–42. [[CrossRef](#)]
22. Abron, A.; Hopfensperger, M.; Thompson, J.; Cooper, L.F. Evaluation of a predictive model for implant surface topography effects on early osseointegration in the rat tibia model. *J. Prosthet. Dent.* **2001**, *85*, 40–46. [[CrossRef](#)]
23. Shahi, S.; Özcan, M.; Maleki Dizaj, S.; Sharifi, S.; Al-Haj Husain, N.; Eftekhari, A.; Ahmadian, E. A review on potential toxicity of dental material and screening their biocompatibility. *Toxicol. Mech. Methods* **2019**, *15*, 1–10. [[CrossRef](#)]
24. Cunha, A.; Elie, A.-M.; Plawinski, L.; Serro, A.P.; Botelho do Rego, A.M.; Almeida, A.; Urdaci, M.C.; Durrieu, M.-C.; Vilar, R. Femtosecond laser surface texturing of titanium as a method to reduce the adhesion of *Staphylococcus aureus* and biofilm formation. *Appl. Surf. Sci.* **2016**, *360*, 485–493. [[CrossRef](#)]
25. Branemark, P.I.; Hansson, B.O.; Adell, R.; Breine, U.; Lindström, J.; Hallén, O.; Ohman, A. Osseointegrated implants in the treatment of the edentulous jaw. Experience from a 10-year period. *Scand. J. Plast. Reconstr. Surg. Suppl.* **1977**, *16*, 1–132.
26. Mavrogenis, A.F.; Dimitriou, R.; Parvizi, J.; Babis, G.C. Biology of implant osseointegration. *J. Musculoskelet. Neuronal Interact.* **2009**, *9*, 61–71.
27. Xiao, J.; Zhou, H.; Zhao, L.; Sun, Y.; Guan, S.; Liu, B.; Kong, L. The effect of hierarchical micro/nanosurface titanium implant on osseointegration in ovariectomized sheep. *Osteoporos. Int.* **2011**, *22*, 1907–1913. [[CrossRef](#)]
28. Wu, S.; Liu, X.; Yeung, K.W.K.; Guo, H.; Li, P.; Hu, T.; Chung, C.Y.; Chu, P.K. Surface nano-architectures and their effects on the mechanical properties and corrosion behavior of Ti-based orthopedic implants. *Surf. Coat. Technol.* **2013**, *233*, 13–26. [[CrossRef](#)]
29. Silverwood, R.K.; Fairhurst, P.G.; Sjöström, T.; Welsh, F.; Sun, Y.; Li, G.; Yu, B.; Young, P.S.; Su, B.; Meek, R.M.; et al. Analysis of osteoclastogenesis/osteoblastogenesis on nanotopographical titania surfaces. *Adv. Healthc. Mater.* **2016**, *5*, 947–955. [[CrossRef](#)]
30. Alonso-Pérez, R.; Bartolomé, J.F.; Ferreira, A.; Salido, M.P.; Pradíes, G. Original vs. non-original abutments for screw-retained single implant crowns: An in vitro evaluation of internal fit, mechanical behaviour and screw loosening. *Clin. Oral Implant. Res.* **2018**, *29*, 1230–1238. [[CrossRef](#)]
31. Shevchenko, A.V.; Dudnik, E.V.; Tsukrenko, V.V.; Ruban, A.K.; Red'ko, V.P.; Lopato, L.M. Microstructural design of bioinert composites in the ZrO_2 - Y_2O_3 - CeO_2 - Al_2O_3 - CoO system. *Powder Metall. Metal Ceram.* **2013**, *51*, 724–733. [[CrossRef](#)]
32. Duan, S.; Shi, X.; Mao, M.; Yang, W.; Han, S.; Guo, H.; Guo, J. Investigation of the Oxidation Behaviour of Ti and Al in Inconel 718 Superalloy During Electroslag Remelting. *Sci. Rep.* **2018**, *8*, 5232. [[CrossRef](#)]

